07,10

Dependence of the superionic transition temperature on the characteristic size and morphology of actinide nanooxides

© A.P. Chernyshev

Institute of Solid State Chemistry and Mechanochemistry, Siberian Branch of the Russian Academy of Sciences, Novosibirsk, Russia
Novosibirsk State Technical University, Novosibirsk, Russia

E-mail: alfred.chernyshev@solid.nsc.ru

Received February 19, 2024
Revised February 19, 2024
Accepted March 15, 2024

The possibility of applying the Bredig rule to determine the temperature of the superionic transition in stoichiometric actinide nanooxides is considered. The comparison of the nanothermodynamic approach with calculations by the method of molecular dynamics is carried out. It is shown that both the morphology and the characteristic size of nanoobjects of actinide dioxides significantly affect the temperature of the superionic transition: the temperature of the superionic transition at a fixed value of the characteristic size of nanoobjects increases in the sequence spherical nanoparticles–nanowires–thin films and decreases with decreasing characteristic size. The possibility of controlling the temperature of the superionic transition in nanoobjects of actinide dioxides is discussed.

Keywords: Nanoparticles of actinide dioxides, nanowires of actinide dioxides, thin films of actinide dioxides, Bredig rule, superionic transition, Lindemann criterion.

DOI: 10.61011/PSS.2024.04.58201.30

1. Introduction

A sharp increase of the ionic conductivity of materials is observed in case of superionic transition. This transition is also referred as the Bredig transition or the λ-transition in the literature. Chemical compounds with the structure of fluorite [1] belong to compounds that undergo transition into the superionic state when heated. Nanoobjects consisting of actinide dioxides AnO_2 are considered (here An — Am, Np, Pa, Pu, Th and U) are considered in this article. These compounds commonly have a fluorite structure (space group $Fm\bar{3}m$). A crystal lattice with a fluorite structure can be considered as a combination of a face-centered cubic sublattice containing An cations and a simple cubic sublattice with oxygen anions. There are experimental data in the literature as well as the data calculated using molecular dynamics (MD) method on the superionic transition in macroscopic ThO_2 [2] and UO_2 [3–5], as well as calculations using the MD method confirming the presence of such a transition in macroscopic PuO_2 [6,7]. There are no experimental or calculated data for the remaining actinide dioxides indicating the presence or absence of a superionic transition in these chemical compounds. It is assumed in this paper that all considered actinide dioxides undergo transition into a superionic state when heated since they have a fluorite structure.

The superionic transition in actinide dioxides at the atomic level can be described as follows. The number of anti-Frenkel defects in the oxygen sublattice consisting of an oxygen vacancy and an interstitial oxygen anion increases with an increase of the temperature. Accordingly, the degree of disorder in the oxygen sublattice increases, while the actinide cations remain in their ideal positions corresponding to the face-centered cubic crystal lattice [1]. The oxygen anions rapidly diffuse through the crystal lattice at temperatures above the superionic transition temperature (T_λ) which causes high ionic conductivity of actinide dioxides in this temperature range [3].

Stoichiometric dioxides of actinides AnO_2 melt congruently, without producing solidus and liquidus lines. For example, stoichiometric thorium dioxide melts congruently, while liquidus and solidus temperatures can be clearly observed in hypostoichiometric oxide already at O/Th = 1.98 [2]. The nature of the transition of actinide dioxides into the superionic state also depends on their stoichiometry [2,3,6–8]. The superionic transition is a λ-type transition for AnO_2 and its temperature is determined by Bredig's rule:

$$T_\lambda(\infty) \approx 0.85 \cdot T_m(\infty), \quad (1)$$

here $T_m(\infty)$ — the melting point of the macroscopic sample. The sign ∞ here and below shows that this value characterizes a macroscopic solid. The transition of hypostoichiometric actinide dioxides AnO_{2-x} into the superionic state is a phase transition of the first kind, the temperature of which depends on x [2,3]. The concentration of defects gradually increases in hyperstoichiometric actinide dioxides AnO_{2+x} with an increase of the temperature, that is, a „diffuse“ transition to a superionic state is observed without, in fact, any sharp phase transition [2,3].

Table 1. Additional physical parameters used to calculate the Bredig temperature of nanoobjects

AnO_2	AmO_2	NpO_2	PaO_2	PuO_2	ThO_2	UO_2
$T_\lambda(\infty)$, K	–	–	–	2320[1] [13] 2350[1] [7] 2100[1] [6]	3091 ± 6 [2], 3040[1] [14]	2670 ± 30 [3,4] 2715 ± 100 [8]
$0.85T_m(\infty)$, K[2]	2028	2611 ± 50	2720 ± 60	2564 ± 28	3103 ± 20	2652 ± 20

Note. [1] MD modeling; [2] according to the formula (1).

The nanothermodynamic method used in this paper makes it possible to study an entire class of compounds almost simultaneously (for example, AnO_2 in the nanoscale of characteristic sizes). At the same time, calculations using the MD method require significant computer time and therefore, as a rule, are performed for nanoparticles of the same shape and the same composition. For instance, the dependence of the melting temperature and the temperature of the superionic transition on the characteristic size of cubic nanoparticles UO_2 was calculated in Ref. [9–11]. The purpose of this paper was to study the dependence of the temperature of the superionic transition on the characteristic size and morphology of stoichiometric actinide nanoxides of different morphologies in a wide range of characteristic sizes using the nanothermodynamic method.

2. Theory

The onset of melting of a substance is characterized by the Lindemann melting criterion [12]. Melting occurs when the following condition is met in accordance with this criterion

$$\sqrt{\langle\sigma^2\rangle} \geq \xi \cdot h, \tag{2}$$

here $\sqrt{\langle\sigma^2\rangle}$ denotes the square root of the atom mean-squared displacement (MSD) from the equilibrium position, ξ — a certain fraction of the interatomic distance h at which melting occurs. The temperature of the superionic transition of actinide dioxides $T_\lambda(\infty)$ can be calculated according to the Bredig's rule (1) or it can be obtained experimentally (Table 1).

The superionic transition of actinide dioxides is accompanied by partial or complete disordering of the oxygen sublattice of their crystal structure, so that it is possible to speak about „melting" of this sublattice [1]. The Bredig's rule gives a one-to-one ratio between $T_m(\infty)$ and $T_\lambda(\infty)$, which indicates that the superionic transition also begins when the Lindemann criterion is met:

$$\sqrt{\langle\sigma^2\rangle_{\text{ox}}} \geq \xi_{\text{ox}} \cdot h. \tag{3}$$

The ox index here indicates that the parameters relate to the oxygen sublattice. This conclusion is confirmed by the results of calculations of the temperature dependence of $\langle\sigma^2\rangle_{\text{ox}}$ ions of the oxygen sublattice of neptunium dioxide [15], plutonium [6] and uranium [16] using the molecular dynamics method. Indeed, calculations showed for UO_2 that $T_\lambda(\infty) \approx 2600$ K (this value practically coincides with the experimental values listed in Table 1) and that the value $\langle\sigma^2\rangle_{\text{ox}}$ grows almost linearly with temperature in the temperature range of 2000−2500 K. A sharp increase of $\langle\sigma^2\rangle_{\text{ox}}$ begins at 2600 K, which is attributable to the beginning of the superionic transition and confirms the applicability of (3) for determining T_λ. The calculation of $\langle\sigma^2\rangle_{\text{ox}}$ and $\langle\sigma^2\rangle$ for the anionic and cationic lattices of NpO_2, respectively, was performed in the temperature range of 300−2000 K, which did not allow the authors of [15] to determine the value of $T_\lambda(\infty)$, since it does not fall within the studied temperature range (Table 1). It follows from the calculations performed using the MD method for PuO_2 in the temperature range of 300−3600 K [6] that a sharp increase of $\langle\sigma^2\rangle_{\text{ox}}$ occurs at a temperature of about 2100 K. This calculated value of the superionic transition temperature in PuO_2 is less than the value obtained using the MD method in Ref. [7,13] (Table. 1) and less than the value obtained using the Bredig's rule (1). The absence of experimental data on the temperature of the superionic transition in PuO_2 does not allow evaluating the reliability of the MD calculations performed in Ref. [6,7,13], therefore, the value $T_\lambda(\infty)$, determined using the Bredig's rule (Table 1), is assumed in this paper. Thus, it follows from the calculations using the MD method [6,16] that the MSD of oxygen anions located in the nodes of the crystal lattice increases faster with an increase of the temperature than the MSD of An cations. Therefore, the Lindemann criterion (3) is satisfied in an oxygen crystal sublattice at a lower temperature than the Lindemann criterion (2) for melting the entire sample, i.e. $T_\lambda(\infty) < T_m(\infty)$.

The dependence $\langle\sigma^2\rangle$ on the characteristic size and morphology of nanoobjects is described by the following phenomenological equation [17]:

$$\langle\sigma^2(\chi + \delta\chi, T)\rangle - \langle\sigma^2(\chi, T)\rangle = (\alpha - 1)\langle\sigma^2(\chi, T)\rangle d\chi, \tag{4}$$

where $\chi = n_s/n_v$, n_s and n_v — the number of surface atoms and the number of atoms located inside the nanoobject, respectively; T — the absolute temperature. In this equation α — the material constant, which can be calculated using the formula [18]:

$$\alpha = \langle\sigma_s^2\rangle/\langle\sigma_v^2\rangle = 1 + 2\Delta S_{\text{vib}}(\infty)/(3R), \tag{5}$$

here the values $\langle\sigma_s^2\rangle$ and $\langle\sigma_v^2\rangle$ refer to surface atoms and atoms, located inside the nanoobject, respectively;

Table 2. Physical parameters

AnO_2	$T_m(\infty)$, [20,21] K	$\Delta H(\infty)$, [21] $kJ \cdot mol^{-1}$	$\Delta S_m(\infty)^1$, $J \cdot mol^{-1} \cdot K^{-1}$	$\Delta S_{vib}(\infty)$, $J \cdot g\text{-}atom^{-1} \cdot K^{-1}$	a, [20] nm	h, (9) nm
AmO_2	2386	–	–	7.7[2]	0.5375 [22]	0.2327
NpO_2	3072 ± 50	70 ± 6	22.8	7.6 ± 0.7	0.54338	0.2353
PaO_2	3200 ± 60	–	–	7.7[2]	0.5446	0.2358
PuO_2	3017 ± 28	64 ± 6	21.2	7.1 ± 0.7	0.53951	0.2336
ThO_2	3651 ± 17	88 ± 6	24.1	8.0 ± 0.6	0.55971	0.2424
UO_2	3120 ± 20	75 ± 3	24.0	7.3 ± 0.3	0.5471 [23]	0.2369

Note. [1] The value of $\Delta S_m(\infty)$ was determined using the formula $\Delta S_m(\infty) = \Delta H_m(\infty)/T_m(\infty)$. [2] Estimation using the average value $\Delta S_m(\infty)$ (see the description in the text).

$\Delta S_{vib}(\infty)$ — the vibrational component of the melting entropy attributed to one gram-atom ΔS_m, R — the universal gas constant.

The melting entropy can be written in the following form [19]:

$$\Delta S_m = \Delta S_{vib} + \Delta S_{conf} + \Delta S_{el}, \quad (6)$$

where ΔS_{conf} and ΔS_{el} — the configuration and electronic entropy, respectively. The contribution of ΔS_{el} to the melting entropy AnO_2 can be neglected, and the value of ΔS_{conf} can be estimated using the formula [19]:

$$\Delta S_{conf} = -R(x_A \ln x_A + x_V \ln x_V), \quad (7)$$

where x_A and x_V —the molar fractions of the base substance and vacancies, respectively, $x_A = 1/(1 + \Delta V/V)$, ΔV — the change of volume of the substance during melting, V — the volume of the substance before melting and $x_V = 1 - x_A$. The formula (7) holds for homogeneous melt. The values ΔV and V were calculated using the density values of uranium dioxide in solid and liquid state at melting point: 9555 and 8860 kg/m^3 [4], respectively. The calculation showed that

$$\Delta S_{conf}(\infty) = 2.167\,J \cdot mol^{-1} \cdot K^{-1}$$

or

$$0.722J \cdot g\text{-}atom^{-1} \cdot K^{-1}.$$

It follows from this that

$$\Delta S_{vib}(\infty) = \Delta S_m(\infty) - \Delta S_{conf}(\infty)$$

$$\approx 7.28\,J \cdot g\text{-}atom^{-1} \cdot K^{-1}.$$

There is no available literature data for other dioxides on density in liquid and solid state at melting point, which did not allow calculating their configuration entropy. Nevertheless, it was assumed for calculations that $\Delta S_{vib}(\infty) \approx (\Delta S_m(\infty)/n$ since the value calculated for UO_2 $\Delta S_{conf}(\infty)$ is close to the error in determining the value of $\Delta S_m(\infty)$ for other AnO_2 (see Table 2). Here n is the number of atoms in a molecule, so the unit of measurement of $\Delta S_{vib}(\infty)$ is $J \cdot g\text{-}atom^{-1} \cdot K^{-1}$ [18]. The melting enthalpies of PaO_2 and AmO_2 are not reported in the literature, therefore, the average value of $\Delta S_m(\infty)$ (according to the data given in Table 2) equal to $23.1\,J \cdot mol^{-1} \cdot To^{-1}$ was taken as the first approximation for AmO_2 and PaO_2.

The parameter χ of spherical and cubic nanoparticles, nanowires and thin films has the following simplest form [24]:

$$\chi = \frac{n_s}{n_v} = (D/D_0 - 1)^{-1}, \quad (8)$$

here D — the characteristic size of nanoobjects (for example, the diameter of spherical nanoparticles and nanowires, the thickness of thin films and the edge length of cubic nanoparticles); $D_0 = 2(3 - d)h$; $d = 0$, 1 and 2 for spherical (or cubic) nanoparticles, nanowires and thin films, respectively. The parameter h for the fluorite structure was defined in [24] as

$$h = \frac{\sqrt{3}}{4}\,a, \quad (9)$$

where a — the lattice constant (Table 2). The solution of the equation (2) gives the dependence $\langle\sigma^2\rangle$ on χ:

$$\langle\sigma^2(\chi)\rangle = \langle\sigma^2(\infty)\rangle \exp[(\alpha - 1)\chi]. \quad (10)$$

The high-temperature approximation can be used since T_m is usually higher than the Debye temperature [17]:

$$\langle\sigma^2(\chi, T)\rangle = \varphi(\chi)T, \quad (11)$$

here $\varphi(\chi)$ is a temperature-independent function χ. Substitution of (11) in (10) gives the following equation:

$$\varphi(\chi) = \varphi(\infty) \exp[(\alpha - 1)\chi]. \quad (12)$$

The ratio $\varphi(\chi) = (\xi h)^2/T_m(\chi)$ follows from (11) and (2) that is fair for nanoobjects at their melting point $T_m(\chi)$. For macroscopic solids ($\chi = \infty$) at $T_m(\infty)$, respectively, we have that $\varphi(\infty) = (\xi h)^2/T_m(\infty)$. Substitution of the last two equations in (10) results in the following ratio between $T_m(\chi)$ and $T_m(\infty)$ [17]:

$$T_m(\chi) = T_m(\infty) \exp(-(\alpha - 1)\chi). \quad (13)$$

Similarly, it is possible to obtain from (10)–(12) and (3) by replacing $T_m(\infty)$ and $T_m(\infty)$ with $T_\lambda(\infty)$ and $T_\lambda(\chi)$, respectively, that

$$T_\lambda(\chi) = T_\lambda(\infty) \exp(-(\alpha - 1)\chi). \quad (14)$$

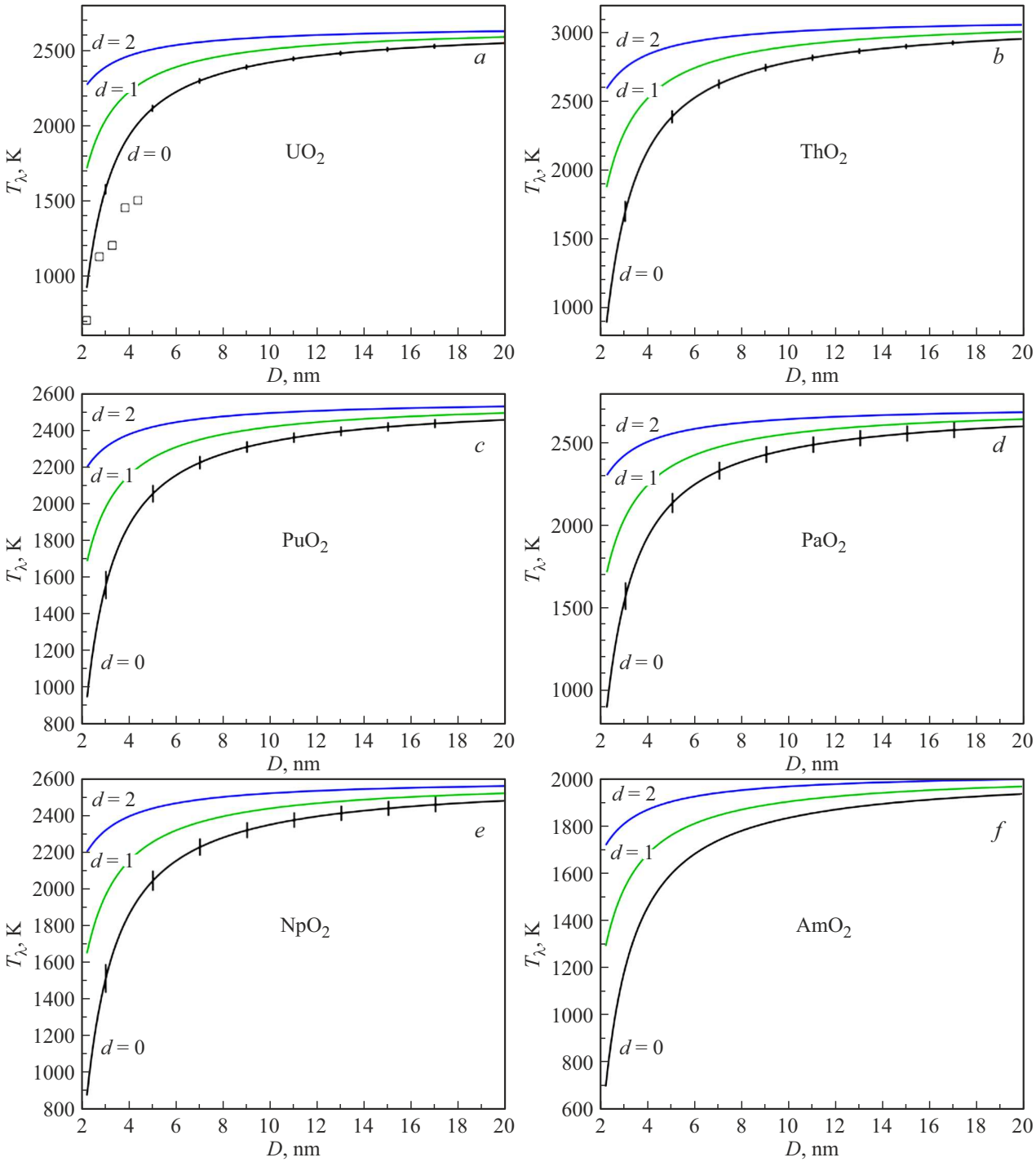

The effect of the size and morphology of nanoobjects on the temperature of the λ-transition (superionic transition): *a* — UO_2, *b* — ThO_2, *c* — PuO_2, *d* — PaO_2, *e* — NpO_2, *f* — AmO_2. Here $d = 0$, 1 and 2 for spherical or cubic nanoparticles, nanowires and thin films, respectively. The square labels are data from [9], which were obtained using MD modeling.

On the other hand, the ratio (14) can be obtained by direct substitution of (13) in (1). It follows from (14) that the temperature of the superionic transition in nanoobjects, as well as their melting point, depends on χ. This conclusion is confirmed by the MD modeling performed in Ref. [9] for cubic nanoparticles. It also follows from (1), (13) and (14) that Bredig's rule is valid not only for macroscopic bodies, but also for nanoobjects within the framework of Lindemann's melting theory.

3. Calculation results and discussion

Calculations of T_λ using ten pair potential sets (PPS) were performed using the MD method in Ref. [10,11].

The values of the superionic transition temperature of cubic nanoparticles of UO_2 were greater or less than the melting point depending on the selected PPS. It should be noted that the first result does not make physical sense for nanoparticles of UO_2. It was found using the MOX-07 PPS that for UO_2 $T_\lambda(\infty) = 2590$ K [10], which practically coincides with the experimental value of this value (Table 1). However, the calculation performed using this PPS showed a very weak dependence of T_λ on the characteristic size of the nanoparticles of UO_2 [10,11]. On the other hand, the MD modeling of the superionic transition in cubic nanoparticles of UO_2, performed in Ref. [9], showed a strong dependence of T_λ on the size of nanoparticles (in the size range of 2.2−5.5 nm, Figure, *a*). The calculations of the superionic transition temperature performed in this paper using the nanothermodynamic method and the results of calculations performed using the MD method in [9] are in good agreement with each other (Figure, *a*). We obtained using the data taken from [9] for calculating the ratio $T_\lambda(D)/T_m(D)$ that this ratio conforms to the Bredig's rule with an underestimated coefficient before T_m:

$$T_\lambda(D) = (0.64 \pm 0.05)T_m(D). \qquad (15)$$

It follows from the calculations using the nanothermodynamic method (Figure) that the superionic transition temperature with a fixed value of the characteristic size of nanoobjects increases in the sequence of spherical nanoparticles-nanowires-thin films (Figure). The difference in T_λ for the considered nanoobjects u decreases as their characteristic size increases. Calculations were performed using formulas (1), (5) and (14), which used tabular data on macroscopic parameters $S_m(\infty)$, $T_m(\infty)$ and $T_\lambda(\infty)$. Therefore, the accuracy of calculations (vertical segments in the figure) is determined by the accuracy of the tabular values used for calculations (Table 1 and 2).

The study conducted in this paper showed that it is possible to change T_λ by changing the morphology and/or the characteristic size of nanoobjects AnO_2. Even with a characteristic size of 20 nm, the difference in the values of T_λ for spherical nanoparticles and thin films is about 100 K (Figure). This difference rapidly grows with a decrease of the characteristic size of nanoobjects and exceeds 500 K with a characteristic size of 3−4 nm. Actinide dioxides having the lowest value of T_m in accordance with Bredig's rule have the lowest value of T_λ. Therefore, AmO_2 has the lowest values of $T_\lambda(D)$ among the studied actinide dioxides (Figure, *f*), and ThO_2 and PaO_2 have the highest values (Figure, *b* and *d* respectively). It should be noted that if nanoobjects are located in a matrix of another substance and have a coherent or semi-coherent boundary with it, then this affects their melting point [24] and, accordingly, may affect T_λ. The impact of the matrix on T_λ was not considered in this paper.

4. Conclusion

Very few studies of the superionic transition in actinide dioxides at the nanoscale have been conducted to date [9–11,25–27]. The results of MD modeling available in the literature are related to the study of T_λ in cubic nanoparticles of UO_2 with a characteristic size from 2.2 to 8.8 nm [9–11] and are contradictory. They strongly depend on the PPS used for modeling, and do not take into account the impact of morphology on T_λ of nanoobjects.

Among the results of MD calculations performed for cubic nanoparticles UO_2 available in the literature [9–11], only the results of [9] allow obtaining an analogue of the Bredig's rule, valid in the nanoscale of characteristic sizes. Theoretical analysis using the nanothermodynamic method performed in this work for UO_2, ThO_2, PuO_2, PaO_2, NpO_2 and AmO_2, as well as MD modeling performed in [9] for cubic nanoparticles of UO_2, showed that the Bredig's rule holds for nanoobjects consisting of actinide dioxides. Therefore, actinide nanodioxides can be used in the superionic state for development of new technologies. The transition temperature of actinide nanodioxides to the superionic state significantly decreases with characteristic sizes less than 10−15 nm (Figure). Calculations performed using the nanothermodynamic method also showed that the superionic transition temperature can be controlled by changing the characteristic size and morphology of nanoobjects of AnO_2.

Conflict of interest

The author declares that he has no conflict of interest.

References

[1] P.C.M. Fossati, A. Chartier, A. Boulle. Front. Chem. **9**, 723507 (1921).
[2] C. Ronchi, J.P. Hiernaut. J. Alloys Compd. **240**, 179 (1996).
[3] J.P. Hiernaut, G.J. Hyland, C. Ronchi. Int. J. Thermophys. **14**, 259 (1993).
[4] International Atomic Energy Agency, Thermophysical properties database of materials for light water reactors and heavy water reactors. Final report of a coordinated research project 1999–2005. Non-serial Publications, IAEA-TECDOC-1496, IAEA, Vienna (2006). 397 p.
[5] M.A. Korneva, S.V. Starikov. Phys. solid state **58**, *1*, 170 (2016). (in Russian).
[6] S.D. Gänay, B. Akgenç. Taşseven. High Temp. Mater. Proc. **35**, *10*, 999 (2016).
[7] D. Bathellier, M. Lainet, M. Freyss, P. Olsson, E. Bourasseau. J. Nucl. Mater. **549**, 152877 (2021).
[8] T.R. Pavlov, M.R. Wenman, L. Vlahovic, D. Robba, R.J.M. Konings, P. Van Uffelen, R.W. Grimes. Acta Materialia **139**, 138 (2017).
[9] R.Yu. Mahmud-Akhunov, M.Yu. Tikhonchev, V.V. Svetukhin. ZhTF **83**, *8*, 8 (2013). (in Russian).
[10] S.I. Potashnikov, A.S. Boyarchenkov, K.A. Nekrasov, A.Ya. Kupryazhkin. J. Nucl. Mater. **419**, 217 (2011).

[11] A.S. Boyarchenkov, S.I. Potashnikov, K.A. Nekrasov, A.Ya. Kupryazhkin. Rasplavy **2**, 32 (2012). (in Russian).
[12] S.S. Batsanov. Zhurn. fiz. khimii **86**, *11*, 1890 (2012). (in Russian).
[13] M.W.D. Cooper, S.T. Murphy, M.J.D. Rushton, R.W. Grimes. J. Nucl. Mater. **461**, 206 (2015).
[14] K. Kobayashi, M. Okumura, H. Nakamura, M. Itakura, M. Machida, M.W.D. Cooper. Sci. Rep. **12**, 9808 (2022).
[15] M. Chollet, J. Leéchelle, R.C. Belin, J.-C. Richaud. J. Appl. Cryst. **47**, 1008 (2014).
[16] H. Zhang, X. Wang, J.F. Douglas. J. Chem. Phys. **151**, 071101 (2019).
[17] F.G. Shi. J. Mater. Res. **9**, 1307 (1994).
[18] Q. Jiang, H.X. Shi, M. Zhao. J. Chem. Phys. **111**, *5*, 2176 (1999).
[19] A.P. Regel, V.M. Glazov. FTP **29**, *5*, 782 (1995). (in Russian).
[20] C. Guéneau, A. Chartier, P. Fossati, L. Van Brutzel, P. Martin. 7.03-Thermodynamic and thermophysical properties of the actinide oxides. In Comprehensive Nuclear Materials. 2nd ed. Elsevier (2020). V. 7. P. 111–154.
[21] R.J.M. Konings, O. Beneš, A. Kovács, D. Manara, D. Sedmidubský, L. Gorokhov, V.S. Iorish, V. Yungman, E. Shenyavskaya, E. Osina. J. Phys. Chem. Ref. Data **43**, 013101 (2014).
[22] E. Epifano, C. Guéneau, R.C. Belin, R. Vauchy, F. Lebreton, J.-C. Richaud, A. Joly, C. Valot, P.M. Martin. Inorg. Chem. **56**, 7416 (2017).
[23] G. Leinders, T. Cardinaels, K. Binnemans, M. Verwerft. J. Nucl. Mater. **459**, 135 (2015).
[24] Q. Jiang, Z. Wen, Thermodynamics of Materials. Higher Education Press, Beijing and Springer-Verlag, Berlin Heidelberg (2011). 300 p.
[25] F. Cappia, D. Hudry, E. Courtois, A. Janßen, L. Luzzi, R.J.M. Konings, D. Manara. Mater. Res. Express **1**, 025034 (2014).
[26] F. Cappia, R. Jovani-Abril, J. Spino, L. Luzzi, A. Janßen, D. Manara. Prog. Nuc. Energ. **72**, 11 (2014).
[27] M. Jin, M. Khafizov, C. Jiang, S. Zhou, C.A. Marianetti, M.S. Bryan, M.E. Manley, D.H. Hurley. J. Phys.: Condens. Matter. **33**, 275402 (2021).

Translated by A.Akhtyamov